An Embedded Network Approach for Scale-Up of Fluctuation-driven Systems

David Cai[(1)], Louis Tao[(2)], and David McLaughlin[(1)]

[(1)] Courant Institute of Mathematical Sciences
New York University
251 Mercer Street, New York, NY 10012

[(2)] Department of Mathematical Sciences
New Jersey Institute of Technology
323 Martin Luther King, Jr., Blvd, Newark, NJ 07102

CAMS Report 0405-26, Spring 2005

Center for Applied Mathematics and Statistics

NJIT

An Embedded Network Approach for Scale-up of Fluctuation-Driven Systems with Preservation of Spike Information

David Cai*[1], Louis Tao‡, and David W. McLaughlin*§

*Courant Institute of Mathematical Sciences &

§Center for Neural Science

New York University, New York, NY 10012

‡Department of Mathematical Sciences, NJIT

Newark, NJ 07102

Abstract To address computational "scale-up" issues in modeling of large regions of the cortex, many coarse-graining procedures have been invoked to obtain effective descriptions of neuronal network dynamics. However, because of local averaging in space and time, these methods do not contain detailed spike information, and, thus, cannot be used to investigate, e.g., cortical mechanisms which are encoded through detailed spike-timing patterns. To retain spike information, we develop a hybrid theoretical framework which embeds a sub-network of point neurons within, and fully interacting with, a coarse-grained network of dynamical background. We employ our newly developed kinetic theory for the description of the coarse-grained background, in combination of a Poisson spike reconstruction procedure to ensure that our method works for the fluctuation-driven regime as well as the mean-driven regime. This embedded network approach is verified to be dynamically accurate and numerically efficient. As an example, we use this embedded representation to construct "reverse-time correlations" as spiked-triggered averages in a ring model of orientation tuning dynamics.

[1]Corresponding author: David Cai, Courant Institute of Mathematical Sciences, New York University, New York, NY 10012. Phone: 212-998-3310, Fax: 212-995-4121, email: cai@cims.nyu.edu.

1 Introduction

Many levels of neuronal representations have been developed in modeling regions of the cortex. Good representations can provide powerful theoretical insights into the workings of the brain and increase significantly our understanding of fundamental cortical mechanisms. However, in computational modelling efforts one immediately confronts crucial issues of "scale-up" in order to model sufficiently large regions of the cortex — for example, to investigate real-world perception and optical illusions in visual cortex. These scale-up issues have been addressed through a hierarchy of reduction and "coarse-graining" steps: simplifying multi-compartment neuron models to fewer compartment models, replacing point neuron representations with more coarse-grained (CG) representations which deal only with spatially/temporally local-averaged quantities, such as mean firing rate [24, 17, 22] and population density representations [11, 1, 4, 7, 18, 13, 14, 9, 5]. Because of local time averaging, detailed information about spikes, such as individual spike timings or interspike interval distributions (ISI), is lost in these CG approaches, including the kinetic theory [5] (which still invokes coarse-graining in time despite its success in describing fluctuation effects). Thus, cortical mechanisms which are encoded through detailed spike-timing patterns cannot be investigated with the present CG techniques.

Here, we introduce a *hybrid framework* which partially retains detailed spike information, yet is numerically efficient and effective for scale-up. The hybridization is accomplished by embedding a sub-network of point-neurons within a CG substrate or background network. This approach is designed to address situations where there exists a biologically distinct sub-network of neurons in interaction with the remaining neuronal population of the substrate. For example, local interactions between point neurons might be represented as a background by local averages in space and time, while sparse (but sufficiently strong) long-range interactions would be represented by a sub-network of the embedded point neurons. Alternatively, a special class of cells might have particularly strong sparse connections, such

as those connecting different cortical layers; or neurons within special cortical regions, such as near orientation pinwheel centers where interaction strengths change so rapidly over short cortical distances that local spatial averaging is not valid, might necessitate the use of embedded neurons. In our approach, we ensure that these two networks (the CG background and the embedded point neurons) can fully interact, with each influencing the other. As they are fully interacting with the CG background, conceptually, these embedded point neurons differ from the notion of "test particles" familiar in physics. Naturally, if the couplings of the embedded network are very sparse and weak, then the embedded neurons reduce to "test neurons" for extracting information about the background.

In the hybrid approach, the level of detail required in modeling of specific neuronal phenomena dictates the specification of particular representations for each of the two networks. For example, for the embedded point neurons, we might invoke an integrate-and-fire (I&F) model, or a more realistic one, such as a Hodgkin-Huxley model. For the CG background, we could use a dynamics of mean firing-rates or population density. In this work, we employ a leaky I&F description for the embedded point neurons, and for the CG background, the kinetic theory [5] which we recently developed to capture fluctuation-dominated network dynamics. We choose this kinetic representation specifically to emphasize that the embedded network method has wide applicability — even for regimes which are driven by fluctuations.

In what follows, this *embedded* representation is developed and its performance is evaluated — its accuracy, efficiency, and numerical effectiveness is established through simulations in comparison with the original I&F networks. We also contrast the kinetic representation with simpler "mean firing rate" representations of the background, demonstrating that in fluctuation-driven regimes, the kinetic theory provides a far more accurate description of the original dynamics than the mean firing rate. We also use the embedded representation to simulate "reverse time correlation" (RTC) experiments which, as spike triggered averages, provide one example in which the retention of spike-timing information is natural. Finally,

we discuss future generalizations and possible applications.

2 Methods

We first coarse-grain a layer of cortex into many, small CG patches as described in [17, 5]. As a specific example, we can take one small CG patch from our large-scale numerical model [12, 23, 21] of the input layer $4C\alpha$ of primary visual cortex (V1) of macaque monkey, which consists of 75% excitatory and 25% inhibitory cells of both simple and complex types[2], represented as I&F point neurons. In [5] we describe an asymptotic reduction of this large-scale point neuron network to a CG kinetic representation which is well suited for scale-up. There, it is shown that this kinetic theory is dynamically accurate and numerically efficient, even when the original point neuron network is fluctuation-dominant. However, the coarse graining procedure in the derivation of the kinetic theory includes a local average over time, thus removing detailed spike-timing information. Here, to regain this spike information, we take the hybrid approach, identifying a distinguished sub-network of point neurons which will be retained, and replacing the other neurons with a CG kinetic description.

Now we turn to the description of the essential steps used in this hybridization procedure. The original I&F dynamics of the i^{th} neuron of a CG patch in the subnetwork to be coarse-grained (as background) is governed by

$$\tau \frac{d}{dt} V_{\alpha i}^{\lambda} = -\left(V_{\alpha i}^{\lambda} - V_R\right) - G_{\alpha i}^{\lambda E}(t)\left(V_{\alpha i}^{\lambda} - V_E\right) - G_{\alpha i}^{\lambda I}(t)\left(V_{\alpha i}^{\lambda} - V_I\right), \tag{1a}$$

$$\sigma_{\lambda'} \frac{d}{dt} G_{\alpha i}^{\lambda\lambda'} = -G_{\alpha i}^{\lambda\lambda'} + \beta_{\alpha}^{\lambda'} f_{\lambda'} \sum_{\mu} \delta\left(t - T_{\alpha i}^{\lambda'\mu}\right) + S_{\alpha}^{\lambda\lambda'} \sum_{\alpha'} \sum_{j \in P_{\alpha' B}^{\lambda'}} \sum_{\mu} \frac{p_{\alpha' j\mu}^{\lambda'}}{N_{\alpha'}^{\lambda'}} \delta\left(t - t_{\alpha' j}^{\lambda'\mu}\right) + \gamma_{\alpha BD}^{\lambda\lambda'}, \tag{1b}$$

[2]Neurons in the visual cortex are classified [10] "simple" or "complex"— with simple cells responding to visual stimulation in an essentially linear fashion (for example, responding to sinusoidally modulated standing gratings at the fundamental frequency, with the magnitude of response sensitive to the spatial phase of the grating pattern) and with complex cells which respond nonlinearly (with a significant second harmonic) in a phase insensitive manner.

where the second term in Eq. (1b) describes the external drive, the third term, the cortico-cortical couplings among neurons in the CG background, and the last term, the feedback from the remaining, embedded neurons. $\lambda, \lambda' = E, I$ label the excitation and inhibition; τ, σ_E, σ_I denote the membrane, excitatory, and inhibitory time scales, respectively; V, the membrane potential; $G^{\lambda E}, G^{\lambda I}$, excitatory and inhibitory conductance; V_R, V_E, V_I, the resting, excitatory, and, inhibitory reversal potentials, respectively; $\alpha = S, C$, label simple and complex cells, respectively. Here, simple and complex cells are modeled by the following network architecture: $\beta_S^E = 1, \beta_C^E = 0$, i.e., simple cells are driven externally with excitatory inputs in addition to their inputs from other cells, while complex cells are not driven externally and receive inputs only from other cortical cells [5]. In our model, for the sake of presentation, one half of the neurons are simple, the other complex, unless otherwise stated. The external input is modeled by a Poisson spike train (the μth spike is indicated by $T_{\alpha i}^{E\mu}$) with strength f_E and rate $\nu_{0E}(t)$. $\beta_\alpha^I \equiv 0$ for completeness. $\gamma_{\alpha BD}^{\lambda\lambda'} = S_{\alpha BD}^{\lambda\lambda'} \sum_{\alpha'} \sum_{j \in \tilde{P}_{\alpha'}^{\lambda'}} \sum_\mu \left(\tilde{N}_{\alpha'}^{\lambda'}\right)^{-1} \tilde{p}_{\alpha'}^{\lambda' j\mu} \delta\left(t - \tilde{t}_{\alpha' j}^{\lambda'\mu}\right)$ are the inputs (feedback) to the neuron of type (λ, α) in the background from the neurons of (λ', α')-type in the embedded subnetwork, which is symbolized by D. $\tilde{N}_\alpha^\lambda$ is the total number of embedded neurons of (λ, α)-type in the subnetwork. N_α^λ is the number of neurons in the population $P_{\alpha B}^\lambda$ of (λ, α)-type, where B stands for the background. $S_\alpha^{\lambda\lambda'}$ denotes the cortico-cortical connection strength from λ'-population to λ-population of α-cell type. $t_{\alpha j}^{\lambda\mu}$ denotes the μ^{th} spike time of the j^{th} neuron in the population of (λ, α)-type. $S_{\alpha BD}^{\lambda\lambda'}$ describes the coupling strength from the embedded subnetwork of λ'-population to the λ-population in the background. The stochastic nature of synaptic connection [8] is modeled by $p_\alpha^{\lambda j\mu}$, which is a Bernoulli random variable upon receiving an action potential (as represented by $t_{\alpha j}^{\lambda\mu}$ in the I&F model): $p_\alpha^{\lambda j\mu} = 1$ with probability p; $p_\alpha^{\lambda j\mu} = 0$ with probability $1 - p$. Note that all the symbols with a tilde stand for the corresponding variables for the subnetwork of embedded point-neurons.

Next, we replace the "background neurons" with a CG kinetic representation: As de-

scribed in [5], the CG kinetic theory studies the evolution of the probability density function (pdf): $\bar{\rho}_\alpha^\lambda(v, g_E, g_I; t) \equiv \mathbb{E}\left[\frac{1}{N_\alpha^\lambda}\sum_{i=1}^{N_\alpha^\lambda}\left\{\delta[v - V_{\alpha i}^\lambda(t)]\delta[g_E - G_{\alpha i}^{\lambda E}(t)]\delta[g_I - G_{\alpha i}^{\lambda I}(t)]\right\}\right]$, where the expectation $\mathbb{E}$ is taken over all realizations of incoming Poisson spike trains $\left\{T_{\alpha i}^{E\mu}\right\}$, and over possible random initial conditions. For example, $\bar{\rho}_S^E(v, g_E, g_I; t)dvdg_Edg_I$ represents the probability that, at time t, a neuron in a simple, excitatory population has voltage $v \in (v, v + dv)$, an excitatory conductance $g_E \in (g_E, g_E + dg_E)$ and an inhibitory conductance $g_I \in (g_I, g_I + dg_I)$. For the marginal and conditional moments $\rho_\alpha^\lambda(v;t) \equiv \int_0^\infty \bar{\rho}_\alpha^\lambda(v, g_E, g_I; t)dg_Edg_I$, $\mu_\alpha^{\lambda E}(v;t) \equiv \int_0^\infty g_E\bar{\rho}_\alpha^\lambda(g_E, g_I|v;t)dg_Edg_I$, and $\mu_\alpha^{\lambda I}(v;t) \equiv \int_0^\infty g_I\bar{\rho}_\alpha^\lambda(g_E, g_I|v;t)dg_Edg_I$, where $\bar{\rho}_\alpha^\lambda(g_E, g_I|v;t)$ is the conditional pdf, i.e., $\bar{\rho}_\alpha^\lambda(v_E, g_E, g_I; t) = \bar{\rho}_\alpha^\lambda(g_E, g_I|v;t)\ \rho_\alpha^\lambda(v;t)$. Upon closure assumptions [5], our CG kinetic theory of the dynamics (1) yields closed equations for $\rho_\alpha^\lambda(v;t), \mu_\alpha^{\lambda E}(v;t)$ and $\mu_\alpha^{\lambda I}(v;t)$:

$$\partial_t\rho_\alpha^\lambda = \partial_v\left\{\zeta\left(v, \mu_\alpha^{\lambda E}, \mu_\alpha^{\lambda I}\right)\rho_\alpha^\lambda\right\}, \tag{2a}$$

$$\partial_t\mu_\alpha^{\lambda E} = -\frac{1}{\sigma_E}\left(\mu_\alpha^{\lambda E} - \bar{g}_\alpha^{\lambda E}(t)\right) + \frac{\sigma_\alpha^{\lambda E\,2}}{\tau\rho_\alpha^\lambda(v)}\,\partial_v\left[(v - V_E)\rho_\alpha^\lambda\right] + \zeta\ \partial_v\mu_\alpha^{\lambda E}, \tag{2b}$$

$$\partial_t\mu_\alpha^{\lambda I} = -\frac{1}{\sigma_I}\left(\mu_\alpha^{\lambda I} - \bar{g}_\alpha^{\lambda I}(t)\right) + \frac{\sigma_\alpha^{\lambda I\,2}}{\tau\rho_\alpha^\lambda(v)}\,\partial_v\left[(v - V_I)\rho_\alpha^\lambda\right] + \zeta\ \partial_v\mu_\alpha^{\lambda I}, \tag{2c}$$

where $\zeta \equiv \zeta\left(v, \mu_\alpha^{\lambda E}, \mu_\alpha^{\lambda I}\right) \equiv \tau^{-1}\left[(v - V_R) + (v - V_E)\,\mu_\alpha^{\lambda E} + (v - V_I)\,\mu_\alpha^{\lambda I}\right]$ and

$$\bar{g}_\alpha^{\lambda\lambda'}(t) \equiv \beta_\alpha^{\lambda'}\nu_{0\lambda'}(t)f_{\lambda'} + S_\alpha^{\lambda\lambda'}\sum_{\alpha'}pm_{\alpha'}^{\lambda'}(t) + S_{\alpha BD}^{\lambda\lambda'}\sum_{\alpha'}p\tilde{m}_{\alpha'}^{\lambda'}(t), \tag{3a}$$

$$\sigma_\alpha^{\lambda\lambda'\,2} \equiv \frac{1}{2\sigma_{\lambda'}}\left[\beta_\alpha^{\lambda'}f_{\lambda'}^2\nu_{0\lambda'}(t) + \left(S_\alpha^{\lambda\lambda'}\right)^2\sum_{\alpha'}\frac{pm_{\alpha'}^{\lambda'}(t)}{N_{\alpha'}^{\lambda'}}\right] + \frac{\left(S_{\alpha BD}^{\lambda\lambda'}\right)^2}{2\sigma_{\lambda'}}\sum_{\alpha'}\frac{p\tilde{m}_{\alpha'}^{\lambda'}(t)}{\tilde{N}_{\alpha'}^{\lambda'}}, \tag{3b}$$

where $\nu_{0\lambda'}(t)$ is the (temporally modulated) rate for the external Poisson spike train for λ'-population, and $m_\alpha^\lambda(t)$ is the average population firing rate per neuron of (λ, α)-type. $\tilde{m}_\alpha^\lambda(t) = \left(\sigma_\lambda\tilde{N}_\alpha^\lambda\right)^{-1}\int^t e^{-\frac{t-s}{\sigma_\lambda}}\sum_{j\in\tilde{P}_{\alpha B}^\lambda}\sum_\mu\tilde{p}_\alpha^{\lambda j\mu}\delta\left(s - \tilde{t}_{\alpha j}^{\lambda\mu}\right)ds$ captures the feedback from the embedded point neurons. These kinetic equations are posed for $V_I \le v \le V_T$, under two point boundary conditions in v which are derived from the fact that the total flux of neurons across firing threshold V_T is equal to the total flux at reset V_R [5].

The dynamics of the remaining, i.e., the embedded neurons is now described by

$$\tau \frac{d}{dt}\tilde{V}_{\alpha i}^{\lambda} = -\left(\tilde{V}_{\alpha i}^{\lambda} - V_R\right) - \tilde{G}_{\alpha i}^{\lambda E}(t)\left(\tilde{V}_{\alpha i}^{\lambda} - V_E\right) - \tilde{G}_{\alpha i}^{\lambda I}(t)\left(\tilde{V}_{\alpha i}^{\lambda} - V_I\right), \tag{4a}$$

$$\sigma_{\lambda'} \frac{d}{dt}\tilde{G}_{\alpha i}^{\lambda\lambda'} = -\tilde{G}_{\alpha i}^{\lambda\lambda'} + \tilde{\beta}_{\alpha}^{\lambda'}\tilde{f}_{\lambda'} \sum_{\mu} \delta\left(t - \tilde{T}_{\alpha i}^{\lambda'\mu}\right) + \tilde{S}_{\alpha}^{\lambda\lambda'} \sum_{\alpha'} \sum_{j \in \tilde{P}_{\alpha' B}^{\lambda'}} \sum_{\mu} \frac{\tilde{p}_{\alpha'}^{\lambda' j\mu}}{\tilde{N}_{\alpha'}^{\lambda'}} \delta\left(t - \tilde{t}_{\alpha' j}^{\lambda'\mu}\right) + \gamma_{\alpha DB}^{\lambda\lambda'}, \tag{4b}$$

where $\gamma_{\alpha DB}^{\lambda\lambda'} = S_{\alpha DB}^{\lambda\lambda'} \sum_{\alpha'} \sum_{\mu} \hat{p}_{\alpha'}^{\lambda'\mu} \delta\left(t - \hat{t}_{\alpha'}^{\lambda'\mu}\right)$ describes the feedback from the CG populations to the embedded neurons. Instead of using merely the average contribution to this feedback as described by the mean rate $pN_{\alpha}^{\lambda} m_{\alpha}^{\lambda}(t)$, we invoke the Poisson assumption and reconstruct stochastic spiking times $\left\{\hat{t}_{\alpha}^{E\mu}\right\}$, and $\left\{\hat{t}_{\alpha}^{I\mu}\right\}$ using the total population rates $pN_{\alpha}^{E} m_{\alpha}^{E}(t)$ and $pN_{\alpha}^{I} m_{\alpha}^{I}(t)$ as the means for these Poisson spike trains — in order to capture spike fluctuations in our hybrid approach. Note that this Poisson spike reconstruction (PSR) automatically accounts for the spike fluctuation in the input via possibly sparse connections from the background, even if the number of neurons in the background is very large. We will demonstrate the significance of this PSR below.

Eqs.(2) and (4) constitute a network of point neurons embedded within, and fully interacting with, a dynamical CG background represented by kinetic theory (2) . The computation effort of this network involves only the simulation of a small number of embedded I&F neurons plus three (1+1)-D partial differential equations for simple and complex cells in the CG background. This allows us to drastically reduce computational cost otherwise needed in the simulation of the original, full I&F network, while retaining spike timing information within the the CG model [5] for scale-up.

3 Results

We have verified our hybrid approach by comparing the embedded network dynamics to a full I&F network with the same underlying network architecture. First, we address accuracy, and present excellent comparison for systems in which different parts of the total network are replaced by the kinetic theory description.

Fig. 1 shows raster plots (spike times for each neuron) for 5 stimulus periods for a single CG patch containing 400 neurons. The raster plot for the full network of I&F neurons is shown in Fig. 1a, with the results for three embedded networks shown in Figs 1b,c,d. In these embedded networks, the eliminated point neurons are replaced by the kinetic theory CG background (Eqs. (2)). Shown in panels (b,c,d) are the spike rasters for the remaining, i.e., embedded I&F neurons, for comparison with the same neurons in the full network (panel a). In panel b (c, respectively), half complex (simple) excitatory cells are described by the kinetic theory, while in panel d, half complex and half simple cells, again all excitatory, are described by the kinetic theory. Even in this case, the firing patterns of the embedded neurons (panel d) agree well with the full I&F network (panel a).

The networks shown in Fig. 1 are operating in a *fluctuation-dominant* regime [5]. This regime can be a natural operating point for cortical networks [20, 2, 17, 6], whether there are external stimuli or not. Our kinetic theory gives a valid, effective reduced description of such situations [5]. Fig. 2 accentuates this point by comparing results for the same full network of 400 neurons as in Fig 1, with those of the CG background of the embedded networks represented by a CG mean firing-rate representation, $m_\alpha^\lambda(t)$, replacing kinetic theory. This mean firing rate background is obtained by solving

$$m_\alpha^\lambda(t) = -\frac{\Gamma_\alpha^\lambda}{\log\left|1 - U_\alpha^\lambda\left(\left\{m_{\alpha'}^{\lambda'}\right\}\right)\right|} \quad \text{for} \quad U_\alpha^\lambda < 1; \quad m_\alpha^\lambda(t) \equiv 0, \quad \text{otherwise;} \tag{5}$$

for $\lambda, \lambda' = E, I$, $\alpha = S, C$, where $\Gamma_\alpha^\lambda = \tau^{-1}\left(1 + \bar{g}_\alpha^{\lambda E} + \bar{g}_\alpha^{\lambda I}\right)$, $U_\alpha^\lambda\left(\left\{m_{\alpha'}^{\lambda'}\right\}\right) = \frac{V_T - V_R}{V_S^{\lambda\alpha} - V_R}$, and $V_S^{\lambda\alpha} = \tau\left(\Gamma_\alpha^\lambda\right)^{-1}\left(V_R + \bar{g}_\alpha^{\lambda E} V_E + \bar{g}_\alpha^{\lambda I} V_I\right)$, where $\bar{g}_\alpha^{\lambda\lambda'}$ are defined in Eq. (3a). (Eq. (5) can be derived [17] from our kinetic theory (2) by taking the limit $N \to \infty$, and $f_\lambda \to 0$, $f_\lambda \nu_{0\lambda} \to$ finite). Figs 2b,c, and d clearly display the inaccuracy of the firing patterns of the remaining embedded neurons when compared to the same neurons in the full I&F network (panel a). In particular, note the complete failure of this mean firing-rate embedding (Figs. 2c,d) to capture the firing of the complex cells in this fluctuation-driven case, while the kinetic theory embedding provides a faithful representation of the firing of these complex

cells as shown in Fig. 1. Fig. 3 further corroborates this point: Shown are dynamic firing rate curves for four representations in comparison with the full I&F network simulations of only simple cells. As clearly shown in Fig. 3, either purely mean-rate representation (as in the approach of [9]), or the hybrid approach using mean-rate only for the CG background, does not yield quantitatively accurate description. We note that results as shown in Figs. 1-3 can also be viewed as the validation of assumptions used in our CG kinetic theory. We will use only kinetic theory (2) below to describe the CG background, instead of Eq. (5).

Our hybrid approach contains a distinct step of capturing the effects of fluctuations in the feedback to the embedded network from the CG background, which is accomplished via the Poisson-spike reconstruction as described above. (PSR is used elsewhere throughout this paper.) Here, we contrast this step to a feedback of only the mean rate computed using the general kinetic theory (2) (*not* Eq. (5)!) without the PSR, i.e., $\gamma_{\alpha DB}^{\lambda\lambda'}$ is replaced by $S_{\alpha DB}^{\lambda\lambda'} \sum_{\alpha'} pN_{\alpha'}^{\lambda'} m_{\alpha'}^{\lambda'}(t)$ in Eq. (4*b*). One might believe that a coupling of the kinetic theory to embedded point neurons through the direct use of this modulated mean firing rate would be just as effective. The results shown in Fig. 4 establish that it is not, i.e., it does not capture the fluctuations well enough for an accurate description. Fig. 4a shows firing rate curves for excitatory complex neurons as a function of the average input conductance $G_{input} = f_E \nu_{0E}$ for steady inputs, while Fig. 4b shows cycle-averaged firing rate under temporally periodically modulated inputs. In both the steady state and dynamically modulated cases (Figs 4a,b), the firing rates of embedded neurons compare quantitatively very well with those of the full I&F network simulation when the PSR is used in combination of kinetic theory, while the modeling error in rate of the embedded approach can be rather substantial without the proper fluctuation effect in the feedback from the CG background. Indeed, PSR is needed in fluctuation-dominated systems.

Having addressed the modeling accuracy issues of the hybrid approach, we turn to demonstration of its full power in modeling situations when there is a sub-network of neurons which

are sparse, yet strongly coupled. Here we consider an idealized network containing such a distinguished sub-network — both to illustrate the necessity of the embedded network to model this situation efficiently, and to contrast with another modeling situation in which "test neurons" within a kinetic theory can provide an adequate description.

The idealized network is comprised of a four population network (complex, simple, excitatory, inhibitory) of 400 neurons. There are only 8 complex cells in this network, forming a distinct sub-network which is very strongly coupled. [Synaptic coupling strengths for these strongly coupled complex cells are $\tilde{S}_C = (0.4, 0.4, 0.8, 0.4)$, in contrast to $S_S = (0.1, 0.2, 0.1, 0.2)$ for the simple cells in the background and $S_{CDB} = (0.25, 0.2, 0.25, 0.2)$, $S_{SBD} = (0.025, 0.05, 0.025, 0.05)$ for the couplings between the sub-network and the CG background.] Fig. 5 displays the dynamics of this network characterized by (i) raster plots, (ii) cross-correlation as quantified by the conditional firing rate, i.e., the probability per unit time that the j^{th} neuron fires, given the condition that the i^{th} neuron fires, averaged over all i and j, and (iii) ISI distributions. These characteristics from the simulation of the full I&F network (lower panels) are successfully reproduced by the hybrid approach (upper panel), when all simple cells are coarse-grained using the kinetic theory and the eight distinct neurons are treated as an embedded network of point neurons. Instead of this constant external stimuli, a more useful and interesting situation for demonstrating the power of the hybrid approach is when the background actually has its own response dynamics to time-dependent stimuli. Here, the hybrid network really shows its ability to capture the distinct dynamics of the strongly interacting embedded subnetwork as demonstrated in the lower panel of Fig. 6. Clearly, in addition to the cross-correlation induced by the external periodic drive (as captured by the test neurons in the upper panel of Fig. 6), the strongly interacting embedded neurons exhibit a stronger cross-correlation with more fine structure, which reflects relatively coherent recurrent dynamics of their own subnetwork. Furthermore, had we used merely test neurons to extract spike information of the embedded network, we would ob-

tain a singled peaked ISI distribution instead of a doubly peaked ISI distribution for the interacting embedded neurons (Fig. 6).

If one merely desires firing statistics of individual neurons *in the background*, test neurons in the embedded subnetwork will extract that information from a background whose full dynamics is modelled by kinetic theory. Fig. 7 shows excellent agreement between the ISI distribution of firing statistics of a sample neuron in a network, obtained by the full I&F network simulation, and that of a test neuron in the CG background description by kinetic theory.

To further illustrate the usefulness of the embedded neurons in the sense of test neurons, we use our hybrid approach to construct a reverse-time correlation (RTC) (Fig. 8). RTC methods enable the experimentalist to probe the dynamical response of a cortical network from a system-analysis viewpoint. Based upon "spike triggered counting," these methods are most directly modelled using detailed spike timing information, thus are natural for the applications of embedded point neuron networks. In one version of these methods [16], the experimentalist sequentially presents an anesthetized monkey with a grating stimulus, chosen randomly at every refresh time T_{refresh} from a collection of grating patterns with varying orientations and spatial phases, and measures the response of an individual cell in V1 extracellularly. For each spike, one asks at time τ earlier, what was the orientation and grating angle of the stimulus pattern presented? Running over all spikes, one measures the probability $P(\theta, \phi; \tau)$ that, at time τ before each spike, the stimulus had orientation θ and spatial phase ϕ. $P(\theta, \phi; \tau)$ provides an estimate of the first-order linear response function of the cortical system.

We have constructed the RTC for neurons on a ring which models the orientation tuning dynamics of primary V1 neurons [19, 15, 13, 5]. The spatial (i.e., angular, here) couplings are described by Gaussian kernels $K_{\lambda\lambda'}(\theta - \theta')$. In the hybrid approach, the kinetic theory now has to be generalized to include multiple angular populations to adequately model the

orientation dynamics, and the coupling among these populations are the generalization of Eq. (3):

$$\bar{g}_{\alpha}^{\lambda\lambda'}(\theta,t) \equiv \beta_{\alpha}^{\lambda'}\nu_{0\lambda'}(\theta,t)f_{\lambda'}(\theta) + pS_{\alpha}^{\lambda\lambda'}\sum_{\alpha'}\int K_{\lambda\lambda'}(\theta-\theta')\, m_{\alpha'}^{\lambda'}(\theta',t)d\theta',$$

$$\sigma_{\alpha}^{\lambda\lambda'}(\theta,t)^2 \equiv \frac{1}{2\sigma_{\lambda'}}\left[\beta_{\alpha}^{\lambda'}f_{\lambda'}^2(\theta)\,\nu_{0\lambda'}(\theta,t) + \left(S_{\alpha}^{\lambda\lambda'}\right)^2\sum_{\alpha'}\int\left[K_{\lambda\lambda'}(\theta-\theta')\right]^2\frac{pm_{\alpha'}^{\lambda'}(\theta',t)}{N_{\alpha'}^{\lambda'}(\theta')}d\theta'\right],$$

which should also be appropriately modified according to Eq. (3) if there are possible inputs from embedded point neurons. Figure 8 shows phase-averaged $P(\theta,\tau) = \int P(\theta,\phi,\tau)\,d\phi$ for a representative simple excitatory cell, computed, respectively, from (i) a network of I&F neurons and (ii) an embedded network of point neurons within a CG background described by the kinetic theory. We obtain an excellent agreement between the result for the full I & F network with those of the embedded network.

4 Discussion

Computational modelling in visual neuroscience faces scale-up issues which must be resolved if the models are to represent regions of the visual cortex of sufficient size to capture most interesting perceptual phenomena. For these purposes one must represent several cortical regions, each with multiple cortical layers of significant lateral extent with their response potentially governed by fluctuations in conductances and voltages. The CG kinetic theory, such as developed in [5], provides a possible resolution of these scale-up problems. However, these CG averaging techniques include a local averaging in time; hence, these methods do not retain detailed spike-timing information of the individual spiking neurons — information which may be needed for certain types of cortical processing.

Here, we have introduced an embedded point neuron representation, benchmarked it for single CG patch, and applied it to an idealized ring model for orientation tuning dynamics. This representation employs the advantages of the CG kinetic theory, while retaining spike-

timing information for an embedded sub-network of point neurons. We have shown that this embedded sub-network approach is both numerically accurate and efficient. It has a wide range over which it can be implemented — from that of an individual "test neuron" to that of a distinguished sub-network of sparse, strongly interacting point neurons, embedded within and fully interacting with the neuronal background described by a CG kinetic theory. However, we note that there might be some limitation to our approach when neurons fire with spike-to-spike synchrony in the background network.

This hybrid network approach can be very useful in a modeling situation in which the neurons in the network fall into distinct biological classes, say, one comprised of neurons which are dense enough that averaging is natural; and the other class comprised of neurons which are sparse (or have sparse synaptic connections), yet with their synapses strong enough that this sparse sub-network fully interacts with the neurons of the other sub-network. Biological possibilities for this sparse sub-network include (i) neurons near positions of rapid change of cortical maps (such as near orientation pinwheel centers); (ii) neurons with long distance connections, which are relatively sparse, yet strong; (iii) neurons and synapses which describe connections between cortical layers; and (iv) neurons of some distinct anatomical type, with strong synapses. In those cases where a strong sparse sub-network is not present, kinetic theory can be used to represent the entire network, together with embedded "test neurons" which captures spike-timing information, useful for modeling of certain important biological measurements, such as RTC.

Finally, another potential advantage of this embedded sub-network approach is that the embedded neurons need not be I&F point neurons. Rather, more realistic models such as Hodgkin-Huxley compartmental models could be used without much loss of numerical efficiency (because of the relatively small number of neurons in the sub-network). We will investigate this possibility in future work.

Acknowledgement D.C. is supported by Sloan Fellowship and by NSF Grants DMS-

0211655 and DMS-0206679. D.W.M is supported by NSF Grant DMS-0211655. L.T. was supported by National Eye Institute T32EY07158.

5 Figure Captions

Figure 1: Comparisons of raster plots of firing dynamics of the original I&F network with networks with different components of the total network replaced by the kinetic theory description — for a single CG patch containing 400 neurons — 200 of which are simple (150 excitatory and 50 inhibitory) and 200 complex (150 excitatory and 50 inhibitory) with network connection probability $p = 0.25$. (We note that our model networks in all figures always have 75% excitatory neurons and 25% inhibitory neurons.) External drive is modeled by Poisson-spike trains with the rate $f\nu_{0E}(t) = 20. \times (1 + 0.5\sin(2\pi f_\omega t))$ with $f_\omega = 10Hz$ and $f = 0.01$, 5 stimulus periods are shown. Network parameters $\sigma_E = 5ms, \sigma_I = 10ms$, $V_R = -70mV, V_T = -55mV$, $V_E = 0mV$, $V_I = -80mV$ (the same for all figures throughout) and $S_S = \left(S_S^{EE}, S_S^{EI}, S_S^{IE}, S_S^{II}\right) = (0.2, 0.4, 0.2, 0.4)$, and $S_C = (0.2, 0.4, 0.2, 0.4)$ (the order convention of $\left(S^{EE}, S^{EI}, S^{IE}, S^{II}\right)$ will be used throughout). In all panels, neurons indexed from 1 to 50 are *simple* excitatory, and 51-100 are *complex* excitatory (inhibitory cells not shown). a) the full network of I&F neurons, b) embedded networks with half of the complex cells coarse-grained; c) embedded network with half of the simple cells coarse-grained; d) the embedded network with half of the simple and half of the complex cells coarse-grained. All CG populations are described by the kinetic theory (Eqs. (2)) with PSR (see text).

Figure 2: Comparisons of raster plots of firing dynamics of the original I&F network with different components of the total network coarse-grained by the mean firing-rate description [Eq. (5)] — for a single CG patch with the same network architecture and parameters as in Fig. 1. In all panels, neurons indexed from 1 to 50 are *simple* excitatory, and 51-100 are *complex* excitatory (inhibitory cells not shown). a) the full network of I&F neurons, b) embedded networks with half of the complex cells coarse-grained; c) embedded network with half of the simple cells coarse-grained; d) the embedded network with half of the simple and half of the complex cells coarse-grained. All coarse-grained populations are described by (Eqs. (5)).

Figure 3: Dynamic firing rate curves for four representations in comparison with the full 400 I&F simple cell network simulations (thick solid line) with network connection probability $p = 0.25$ — (i) All excitatory and inhibitory cells are coarse-grained using our kinetic theory (Eq. (2)) (thin solid line), (ii) All excitatory and inhibitory cells are coarse-grained using the mean firing-rate representation (5) (dotted line); (iii) All inhibitory cells are coarse-grained using the kinetic theory and the excitatory cells are modeled as embedded I&F neurons (thick dashed line); (iv) All inhibitory cells are coarse-grained using the mean firing-rate representation (5) and the excitatory cells are modeled as embedded I&F neuron (thin dashed line). The external drive is modeled by Poisson spike trains with the rate $f\nu_{0E}(t) = 13. \times (1 + 0.25\sin(2\pi f_\omega t)$, $f_\omega = 10Hz$ and $f = 0.01$.

Figure 4: (panel **a**) Steady state firing rate curves as a function of the average input conductance and (panel **b**) cycle-averaged firing rate curves for the embedded, excitatory complex cells in a four population model with both excitatory and inhibitory cells of simple and complex types in comparison with the full I&F simulations (thick solid) of 400 neurons with network connection probability $p = 0.25$. Half of the simple cells are coarse-grained using the kinetic theory (2) with the Poisson spike reconstruction in the feedback to the embedded point-neurons (thin solid), in contrast to the case where only the mean rate from the kinetic theory (2) is used in the feedback (dashed). The external drive is modeled by Poisson spike trains with the rate $f\nu_{0E}(t) = 13. \times (1 + 0.5\sin(2\pi f_\omega t)$, $f_\omega = 10Hz$ and $f = 0.02$. Cycle-averaged firing rate is the rate averaged many periods of the stimulus at $10Hz$ by $m(t) = \sum_{n=1}^{N_t} m(t + nT)/N_t$ for $0 < t < T$, where T is the period.

Figure 5: Dynamics of strongly coupled embedded sub-network on a background under a *constant* external stimulus. Plotted are (i) Raster plots — only the eight complex cells in the distinct sub-population are shown (Neurons labeled 1-6 are excitatory, while labeled 7-8, inhibitory), (ii) Cross-correlation (see text), and (iii) ISI distributions. Lower panels: the simulation of the full I&F network; Upper panels: the hybrid approach when all cells in the

background are coarse-grained using the kinetic theory and the eight distinct complex cells are treated as an embedded network of point neurons.

Figure 6: Dynamics of strongly coupled embedded sub-network on a background driven by a *time-dependent* stimulus. Plotted are (i) Raster plots — only the eight complex cells in the distinct sub-population are shown (Neurons labeled 1-6 are excitatory while labeled 7-8, inhibitory) , (ii) Cross-correlation, and (iii) ISI distributions. Lower panels: the hybrid approach when all cells in the background are coarse-grained using the kinetic theory and the eight distinct complex cells are treated as an embedded network of point neurons; Upper panels: a sub-network of eight *test neurons* in interaction with the background but without interaction among themselves. The external drive is modeled by Poisson spike trains with the rate $f\nu_{0E}(t) = 20. \times (1 + 0.25\sin(2\pi f_\omega t)$, $f_\omega = 1Hz$ and $f = 0.01$.

Figure 7: Extract ISI distributions of neurons in the background — test neuron method. Left: test neuron driven by a CG neuronal patch described the kinetic theory; Right: sample neuron from a full network of I&F neurons. We note that the firing rate of the neuron in the full I&F network is 46 spikes/sec while the test neuron driven by the CG background has 45 spikes/sec — with only a 2% of relative error.

Figure 8: Reverse-time correlation for a simple cell in a ring model for the orientation tuning dynamics of V1 neurons. The LGN is modeled by $\nu_{LGN}(t) = \int dsG_{LGN}(t-s)$ $A_{LGN}(\theta, \phi, \theta_s(s), \phi_s(s))$ with $G_{LGN}(t) = c_0 t^5 \left[\exp(-t/\tau_0) - c_1 \exp(-t/\tau_1))\right], \tau_0 = 3ms, \tau_1 = 5ms, c_0 = 1, c_1 = (\tau_0/\tau_1)^6$, and $A_{LGN}(\theta, \phi, \theta_s(s), \phi_s(s)) = \nu_0 \left[1 + \varepsilon \exp\left(-\frac{(\theta-\theta_s)^2}{2\pi^2 L_{input}^2}\right) \sin(\phi - \phi_s)\right]$, $\varepsilon = 1$, $L_{input} = 0.25$, $f\nu_0 = 10$ [3]. The flash rate of the external patterns is $100Hz$. Left: RTC obtained from an I&F network simulation of the ring model; Right: RTC obtained by coarse-graining all complex cells in the ring model using the kinetic equation.

References

[1] L. Abbott and C. van Vreeswijk. Asynchronous states in a network of pulse-coupled oscillators. *Phys. Rev. E*, 48:1483–1490, 1993.

[2] J. Anderson, I. Lampl, D. Gillespie, and D. Ferster. The contribution of noise to contrast invariance of orientation tuning in cat visual cortex. *Science*, 290:1968–1972, 2000.

[3] E. Benardete and E. Kaplan. The dynamics of primate M retinal ganglion cells. *Vis. Neurosci.*, 16:355–368, 1999.

[4] N. Brunel and V. Hakim. Fast global oscillations in networks of integrate-and-fire neurons with low firing rates. *Neural Comp.*, 11:1621–1671, 1999.

[5] D. Cai, L. Tao, M. Shelley, and D. McLaughlin. A new kinetic representation of fluctuation-driven neuronal networks with application to simple & complex cells in primary visual cortex. *Proc. Natl. Acad. Sci. USA*.

[6] N. Fourcaud and N. Brunel. Dynamics of the firing probability of the noisy integrate-and-fire neuron. *Neural Comp.*, 14:2057–2110, 2002.

[7] W. Gerstner. Population dynamics of spiking neurons: fast transients, asynchronous states, and locking. *Neural Comp.*, 12:43–89, 2000.

[8] N. R. Hardingham and A. U. Larkman. The reliability of excitatory synaptic transmission in slices of rat visual cortex *in vitro* is temperature dependent. *J. Physiol.*, 507:249–256, 1998.

[9] E. Haskell, D.Q. Nykamp, and D. Tranchina. Population density methods for large-scale modelling of neuronal networks with realistic synaptic kinetics: cutting the dimension down to size. *Network*, 12:141–0174, 2001.

[10] D. Hubel and T. Wiesel. Receptive fields, binocular interaction and functional architecture of the cat's visual cortex. *J. Physiol. (Lond)*, 160:106–154, 1962.

[11] B.W. Knight. Dynamics of encoding in a population of neurons. *J. Gen. Physiol.*, 59:734–766, 1972.

[12] D. McLaughlin, R. Shapley, M. Shelley, and J. Wielaard. A neuronal network model of macaque primary visual cortex (V1): Orientation selectivity and dynamics in the input layer $4C\alpha$. *Proc. Natl. Acad. Sci. USA*, 97:8087–8092, 2000.

[13] D. Nykamp and D. Tranchina. A population density method that facilitates large-scale modeling of neural networks: Analysis and application to orientation tuning. *J. Comp. Neurosci.*, 8:19–50, 2000.

[14] D. Nykamp and D. Tranchina. A population density method that facilitates large-scale modeling of neural networks: Extension to slow inhibitory synapses. *Neural Comp.*, 13:511–546, 2001.

[15] M. Pugh, D. Ringach, R. Shapley, and M. Shelley. Computational modeling of orientation tuning dynamics in V1 neurons. *J. Comp. Neuroscience*, 8:143–159, 2000.

[16] D. Ringach, M. Hawken, and R. Shapley. Dynamics of orientation tuning in macaque primary visual cortex. *Nature*, 387:281–284, 1997.

[17] M. Shelley and D. McLaughlin. Coarse-grained reduction and analysis of a network model of cortical response. I. drifting grating stimuli. *J. Comp. Neurosci.*, 12:97–122, 2002.

[18] L. Sirovich, A. Omurtag, and B. Knight. Dynamics of neuronal populations; the equilibrium solution. *SIAM J. Appl. Math.*, 60:2009–2028, 2000.

[19] D. Somers, S. Nelson, and M. Sur. An emergent model of orientation selectivity in cat visual cortical simple cells. *J. Neurosci.*, 15:5448–5465, 1995.

[20] E.A. Stern, A.E. Kincaid, and C.J. Wilson. Spontaneous subthreshold membrane potential fluctuations and action potential variability of rat corticostriatal and striatal neurons in vivo. *J. Neurophysiol.*, 77:1697–1715, 1997.

[21] L. Tao, M. Shelley, D. McLaughlin, and R. Shapley. An egalitarian network model for the emergence of simple and complex cells in visual cortex. *PNAS*, 2003.

[22] A. Treves. Mean field analysis of neuronal spike dynamics. *Network*, 4:259–284, 1993.

[23] J. Wielaard, M. Shelley, R. Shapley, and D. McLaughlin. How Simple cells are made in a nonlinear network model of the visual cortex. *J. Neuroscience*, 21:5203–5211, 2001.

[24] H. Wilson and J. Cowan. A mathematical theory of the functional dynamics of cortical and thalamic nervous tissue. *Kybernetik*, 13:55–80, 1973.

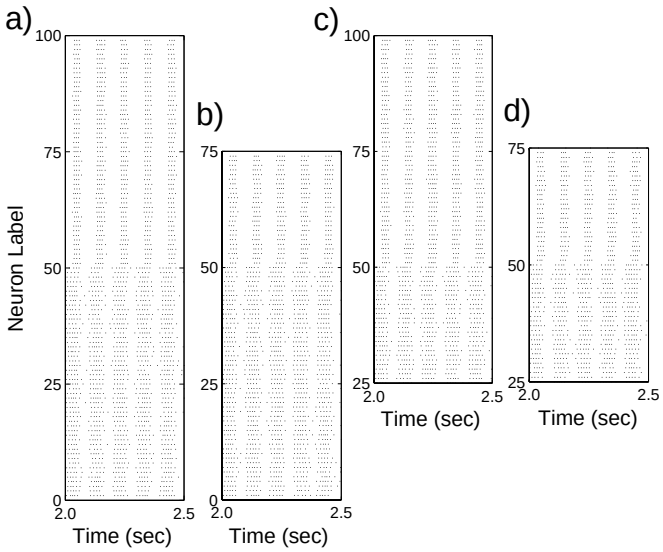

Figure 1: Comparisons of raster plots of firing dynamics of the original I&F network with networks with different components of the total network replaced by the kinetic theory description — for a single CG patch containing 400 neurons — 200 of which are simple (150 excitatory and 50 inhibitory) and 200 complex (150 excitatory and 50 inhibitory) with network connection probability $p = 0.25$. (We note that our model networks in all figures always have 75% excitatory neurons and 25% inhibitory neurons.) External drive is modeled by Poisson-spike trains with the rate $f\nu_{0E}(t) = 20. \times (1 + 0.5\sin(2\pi f_\omega t))$ with $f_\omega = 10Hz$ and $f = 0.01$, 5 stimulus periods are shown. Network parameters $\sigma_E = 5ms, \sigma_I = 10ms$, $V_R = -70mV, V_T = -55mV$, $V_E = 0mV$, $V_I = -80mV$ (the same for all figures throughout) and $S_S = \left(S_S^{EE}, S_S^{EI}, S_S^{IE}, S_S^{II}\right) = (0.2, 0.4, 0.2, 0.4)$, and $S_C = (0.2, 0.4, 0.2, 0.4)$ (the order convention of $\left(S^{EE}, S^{EI}, S^{IE}, S^{II}\right)$ will be used throughout). In all panels, neurons indexed from 1 to 50 are *simple* excitatory, and 51-100 are *complex* excitatory (inhibitory cells not shown). a) the full network of I&F neurons, b) embedded networks with half of the complex cells coarse-grained; c) embedded network with half of the simple cells coarse-grained; d) the embedded network with half of the simple and half of the complex cells coarse-grained. All CG populations are described by the kinetic theory (Eqs. (2)) with PSR (see text).

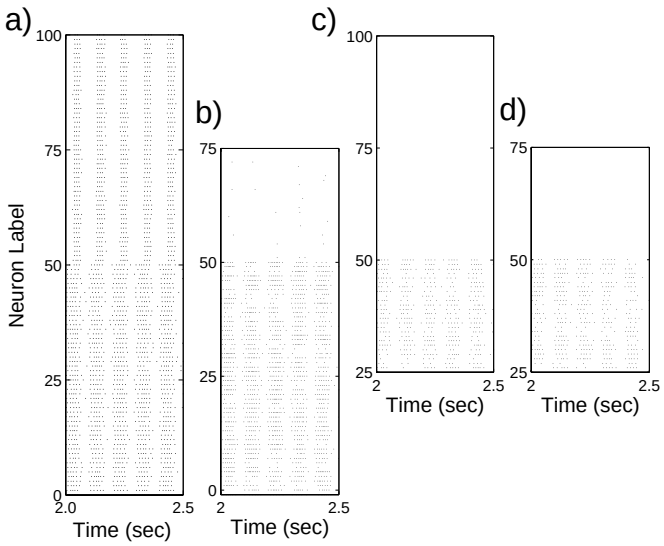

Figure 2: Comparisons of raster plots of firing dynamics of the original I&F network with different components of the total network coarse-grained by the mean firing-rate description [Eq. (5)] — for a single CG patch with the same network architecture and parameters as in Fig. 1. In all panels, neurons indexed from 1 to 50 are *simple* excitatory, and 51-100 are *complex* excitatory (inhibitory cells not shown). a) the full network of I&F neurons, b) embedded networks with half of the complex cells coarse-grained; c) embedded network with half of the simple cells coarse-grained; d) the embedded network with half of the simple and half of the complex cells coarse-grained. All coarse-grained populations are described by (Eqs. (5)).

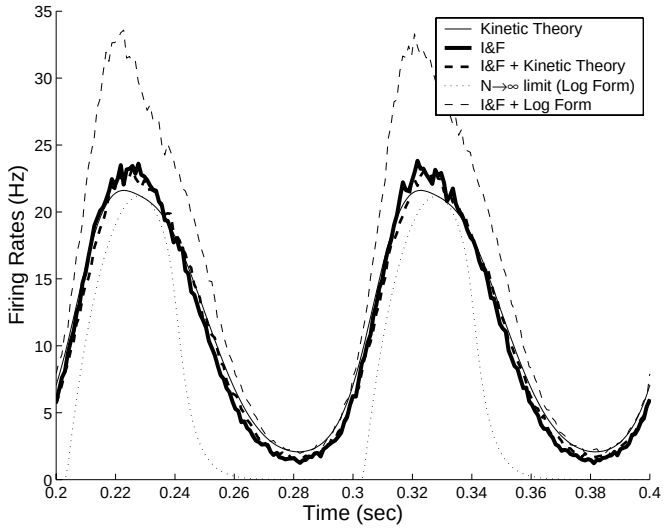

Figure 3: Dynamic firing rate curves for four representations in comparison with the full 400 I&F simple cell network simulations (thick solid line) with network connection probability $p = 0.25$ — (i) All excitatory and inhibitory cells are coarse-grained using our kinetic theory (Eq. (2)) (thin solid line), (ii) All excitatory and inhibitory cells are coarse-grained using the mean firing-rate representation (5) (dotted line); (iii) All inhibitory cells are coarse-grained using the kinetic theory and the excitatory cells are modeled as embedded I&F neurons (thick dashed line); (iv) All inhibitory cells are coarse-grained using the mean firing-rate representation (5) and the excitatory cells are modeled as embedded I&F neuron (thin dashed line). The external drive is modeled by Poisson spike trains with the rate $f\nu_{0E}(t) = 13. \times (1+0.25\sin(2\pi f_\omega t)$, $f_\omega = 10Hz$ and $f = 0.01$.

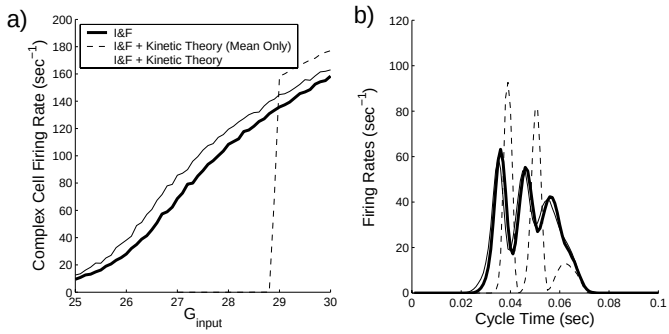

Figure 4: (panel **a**) Steady state firing rate curves as a function of the average input conductance and (panel **b**) cycle-averaged firing rate curves for the embedded, excitatory complex cells in a four population model with both excitatory and inhibitory cells of simple and complex types in comparison with the full I&F simulations (thick solid) of 400 neurons with network connection probability $p = 0.25$. Half of the simple cells are coarse-grained using the kinetic theory (2) with the Poisson spike reconstruction in the feedback to the embedded point-neurons (thin solid), in contrast to the case where only the mean rate from the kinetic theory (2) is used in the feedback (dashed). The external drive is modeled by Poisson spike trains with the rate $f\nu_{0E}(t) = 13. \times (1 + 0.5\sin(2\pi f_\omega t)$, $f_\omega = 10Hz$ and $f = 0.02$. Cycle-averaged firing rate is the rate averaged many periods of the stimulus at $10Hz$ by $m(t) = \sum_{n=1}^{N_t} m(t+nT)/N_t$ for $0 < t < T$, where T is the period.

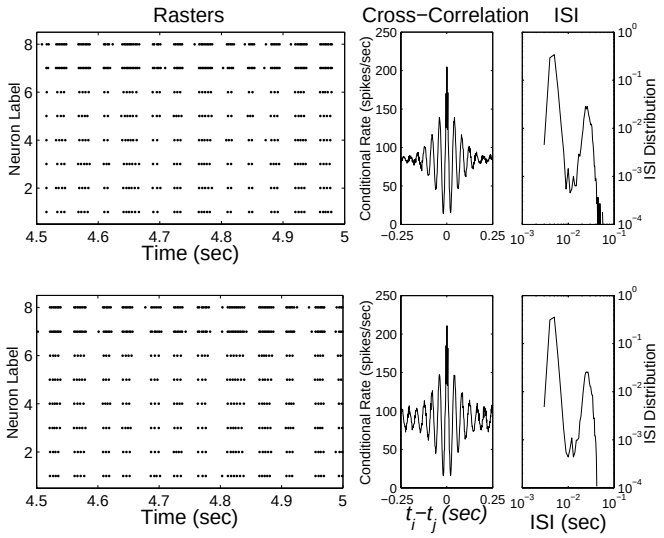

Figure 5: Dynamics of strongly coupled embedded sub-network on a background under a *constant* external stimulus. Plotted are (i) Raster plots — only the eight complex cells in the distinct sub-population are shown (Neurons labeled 1-6 are excitatory, while labeled 7-8, inhibitory), (ii) Cross-correlation (see text), and (iii) ISI distributions. Lower panels: the simulation of the full I&F network; Upper panels: the hybrid approach when all cells in the background are coarse-grained using the kinetic theory and the eight distinct complex cells are treated as an embedded network of point neurons.

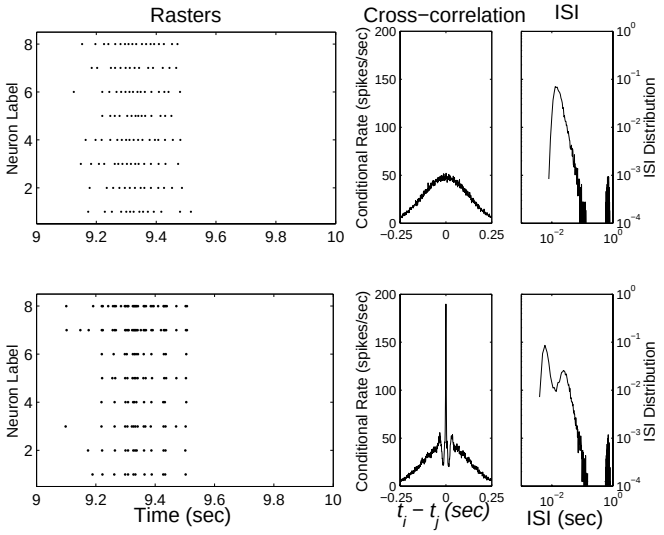

Figure 6: Dynamics of strongly coupled embedded sub-network on a background driven by a *time-dependent* stimulus. Plotted are (i) Raster plots — only the eight complex cells in the distinct sub-population are shown (Neurons labeled 1-6 are excitatory while labeled 7-8, inhibitory) , (ii) Cross-correlation, and (iii) ISI distributions. Lower panels: the hybrid approach when all cells in the background are coarse-grained using the kinetic theory and the eight distinct complex cells are treated as an embedded network of point neurons; Upper panels: a sub-network of eight *test neurons* in interaction with the background but without interaction among themselves. The external drive is modeled by Poisson spike trains with the rate $f\nu_{0E}\,(t) = 20. \times (1 + 0.25\sin(2\pi f_\omega t)$, $f_\omega = 1Hz$ and $f = 0.01$.

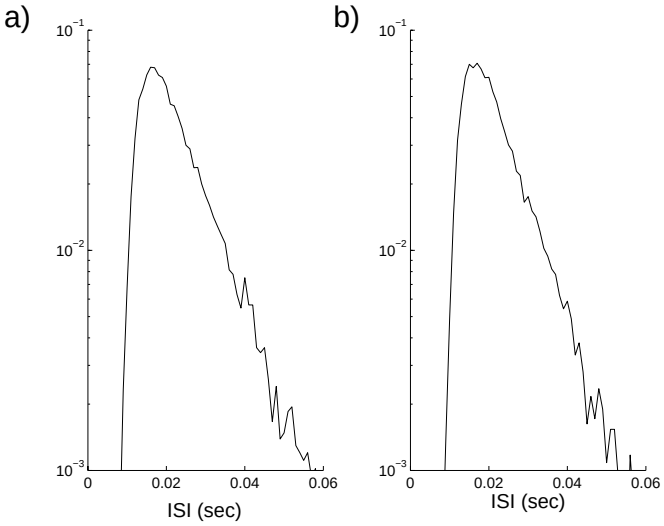

Figure 7: Extract ISI distributions of neurons in the background — test neuron method. Left: test neuron driven by a CG neuronal patch described the kinetic theory; Right: sample neuron from a full network of I&F neurons. We note that the firing rate of the neuron in the full I&F network is 46 spikes/sec while the test neuron driven by the CG background has 45 spikes/sec — with only a 2% of relative error.

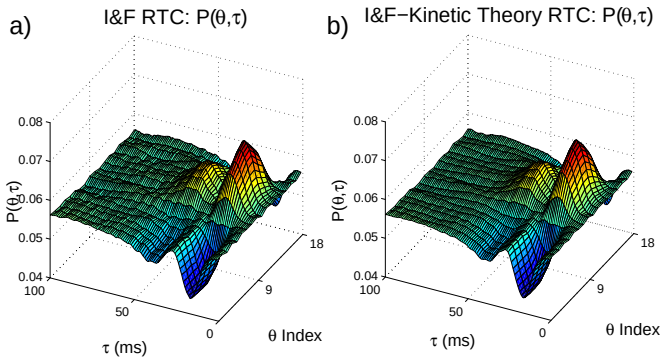

Figure 8: Reverse-time correlation for a simple cell in a ring model for the orientation tuning dynamics of V1 neurons. The LGN is modeled by $\nu_{LGN}(t) = \int ds G_{LGN}(t-s)\ A_{LGN}(\theta,\phi,\theta_s(s),\phi_s(s))$ with $G_{LGN}(t) = c_0 t^5 \left[\exp(-t/\tau_0) - c_1 \exp(-t/\tau_1)\right], \tau_0 = 3ms, \tau_1 = 5ms, c_0 = 1, c_1 = (\tau_0/\tau_1)^6$, and $A_{LGN}(\theta,\phi,\theta_s(s),\phi_s(s)) = \nu_0 \left[1 + \varepsilon \exp\left(-\frac{(\theta-\theta_s)^2}{2\pi^2 L_{input}^2}\right) \sin(\phi - \phi_s)\right]$, $\varepsilon = 1$, $L_{input} = 0.25$, $f\nu_0 = 10$ [3]. The flash rate of the external patterns is $100Hz$. Left: RTC obtained from an I&F network simulation of the ring model; Right: RTC obtained by coarse-graining all complex cells in the ring model using the kinetic equation.